Conjugate Heat Transfer Analysis of an Internally Cooled Gas Turbine Vane

S. I. Kim (a), L. Lebel* (a), S. Sreekanth (b), and H. Ozem (b)
(a) Pratt & Whitney Canada, Longueuil QC
**Presenter and contact author: Larry.Lebel@pwc.ca, (450) 677-9411*
(b) Pratt & Whitney Canada, Mississauga ON

Abstract

A conjugate heat transfer (CHT) method was used to perform the aerothermal analysis of an internally cooled turbine vane, and was validated against experimental and empirical data.

Firstly, validation of the method with regard to internal cooling was done by reproducing heat transfer test data in a channel with pin fin heat augmenters, under steady constant wall temperature. The computed Nusselt numbers for the two tested configurations (full length circular pin fins attached to both walls and partial pin fins attached to one wall only) showed good agreement with the measurements. Sensitivity to mesh density was evaluated under this simplified case in order to establish mesh requirements for the analysis of the full component.

Secondly, the CHT method was applied onto a turbine vane test case from an actual engine. The predicted vane airfoil metal temperature was compared to the measured thermal paint data and the in-house empirical predictions. The CHT results agreed well with the thermal paint data and showed better prediction than the current empirical modeling approach.

Introduction

The thermal efficiency and power density of a gas turbine engine depend significantly on the operating pressure ratio and turbine inlet temperature. The thermal efficiency increases ideally up to stoichiometric turbine inlet temperature, which however is higher than the melting temperatures of turbine airfoil alloys. To allow increases in gas temperature while maintaining desired metal temperatures, cooling schemes relying on various heat augmentation devices have been employed in modern turbine airfoils. Heat transfer augmentation and thermal performance parameters provided by various devices in turbine airfoils, including rib turbulators, pin fins, dimples, and surface roughness, have been compared and systematically reviewed [1].

Internally cooled first stage vane airfoils typically have an insert through which the cooling air is fed (Figure 1). Jets from the holes of this insert generate impingement cooling around the airfoil leading edge. The flow splits thereafter into two channels on both sides of the insert, before it merges again and leaves the airfoil at its trailing edge. The channels on the sides and downstream of the insert are augmented with pin fins.

The flow field inside this internal cooling pattern is complex, and dominated by secondary flows generated by the impingement, turns and pin fins. Observation of such a flow structure is difficult or impossible in the traditional experimental studies. Understanding the fluid flow and associated heat transfer is of importance for precise determination of the metal temperature, which is required to assess the airfoil life with adequate accuracy.

A conjugate heat transfer (CHT) method allows a detailed prediction of both temperature and heat transfer distribution inside the part, and gives an insight into the flow field. Recently, CHT analyses have provided reasonable results and have been applied to realistic vanes and blades with film cooling and serpentine internal passages [2-4]. There have been increased research efforts in improving the accuracy of the CHT methodology with regard to turbulence models [5-6].

The present work is an attempt to apply CHT analysis on the actual first stage turbine vane of an aero engine under its actual operating conditions. The computational methodology was first partly validated by reproducing measured heat transfer data in an internal cooling passage with circular pin fins, before being applied to the actual turbine vane. The predicted vane metal temperature was evaluated against measured thermal paint data and current empirical design tool prediction.

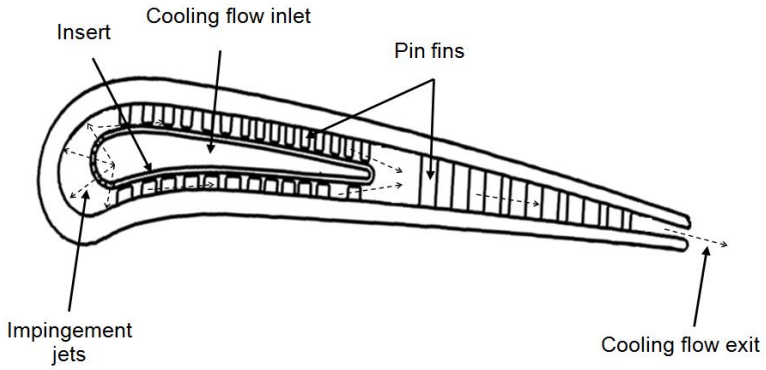

Figure 1: Typical vane airfoil cooling scheme.

Computational Methodology

The physical domain was divided into two different domains: fluid and solid. The steady, compressible, three-dimensional Navier-Stokes equations were solved in the fluid domain, while the Fourier equation for heat conduction was solved in the solid domain. In this CHT method, at the fluid-solid interfaces, an energy balance is satisfied at every iteration, such that the heat flux at the wall on the fluid side is equal in magnitude and opposite sign to the heat flux on the solid side. Thus, all fluid-solid interfaces are fully coupled and required no user-specified boundary values.

The computations were performed using the commercial CFD code ANSYS CFX® V.11 with unstructured meshes. The numerical scheme works on the basis of an implicit element-based finite volume method. The second order advection scheme was selected to calculate the advection terms in the discrete finite volume equations for continuity, energy and momentum. The turbulence transport equations were discretized using the first order upwind scheme [8]. The turbulence closure was provided by the Shear Stress Transport (SST) two-equation turbulence model. The details of the turbulence equations, functions, and constants are available in reference [8].

Surface roughness typically leads to an increase in turbulence production near the wall. This can result in significant increases in wall shear stress and wall heat transfer. Proper modelling of the surface roughness effects is required for a good agreement with heat transfer experimental data. For rough walls, the logarithmic profile still exists, but moves closer to the wall. The roughness height is specified as the equivalent sand grain roughness in ANSYS CFX [8], on the boundaries of a fluid domain that interface with a solid domain.

The grid was generated using the commercial grid generation code ANSYS ICEM CFD^{TM} V.11. Initially, a surface mesh was generated with imposing the maximum triangle size on each surface. The volume was then populated with tetrahedral cells using the Delaunay mesh algorithm with the growth rate from the surface mesh set to 1.2. On the solid walls, fifteen layers of prism elements were finally created with an exponential growth rate of 1.3. To provide adequate resolutions near the walls, a wall coordinate y^+ was maintained less than 1. A grid-refinement study was performed, and is discussed in the next section.

Validation of Channel Flow with Pin Fins

Test case description

For validation purpose, the current method was applied to the pin fin heat augmented cooling passage that was experimentally investigated by Arora and Abdel-Messeh [7]. Both partial length and full length circular pin fins were analysed, in a channel with cross section aspect ratio of 25:1, under constant wall and pin fin temperature condition (71 ℃). The full channel length was modeled, including the entrance and exit channels with lengths of 50 and 16 hydraulic diameters, respectively. As per the experiment, the entrance duct was heated to the same temperature as the test section, in order to obtain a fully developed thermal boundary layer in addition to the fully-developed velocity profile. A total number of ten rows of pin fins were mounted onto ten channel segments, all heated individually to maintain constant temperature, with the amount of heat being monitored.

Following the nomenclature of Figure 2, the selected test case for analysis had axial X/D and lateral S/D pitches of the pins of 2.83 and 2.42, respectively. The pin height to diameter H/D ratio was 1.07 (where H is the distance between the top and bottom walls). For the single sided partial pins, the gap ratio G/H was 0.15 and 0.47. Other details of the test case can be found in reference [7].

Boundary conditions

Reynolds numbers from 3,000 to 25,000, based on pin diameter and velocity in the minimum passage area between pins, were selected for the simulations. A mass flow rate was imposed at the inlet to match the desired Reynolds number, with a temperature of 27 ℃ and a turbulence intensity of 5%. The exit was set to atmospheric pressure.

Computational grid

As the accuracy of solution strongly depends on the quality of the grid, a grid refinement study was performed. The properties of the three tested grids are summarized in Table 1. Partial view of the G1 grid for the case of partial pin fins is shown in Figure 3. The resulting distributions of local Nusselt numbers are shown in Figure 4 for each of the three grids, again with the partial pin geometry. In this figure, the "rough" wall is the bottom one, which supports the pins, whereas the "smooth" wall is the top one, which does not contact the pins. The Nusselt numbers over the rough wall are almost identical between grids G2 and G3. The maximum grid dependence is observed on the smooth wall, with about 10% difference in Nusselt number between G1 and G3 grids.

In conclusion, grid parameters G1 were selected for further analysis of channels with full pin fins, whereas for partial pin fins, where small gaps are present between the pins and the smooth wall, grid parameters G2 were selected. Meshing of the turbine vane case presented later used a combination of those two grid systems.

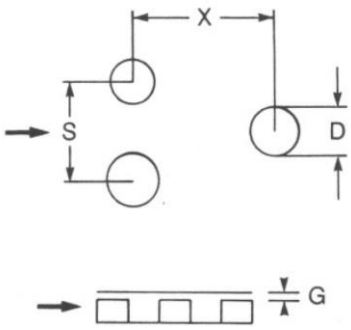

Figure 2: Pin fin array nomenclature.

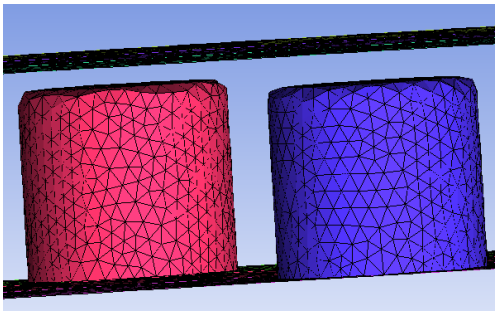

Figure 3: Computational grid G1 for the case of partial pin fins.

Table 1 – Properties of the tested grids

Grid	S_{wall} / D	S_{pin} / D	Number of nodes
G1	0.167	0.083	3,945,897
G2	0.107	0.053	7,877,979
G3	0.083	0.042	10,806,626

S: maximum size of the triangle
D: pin diameter

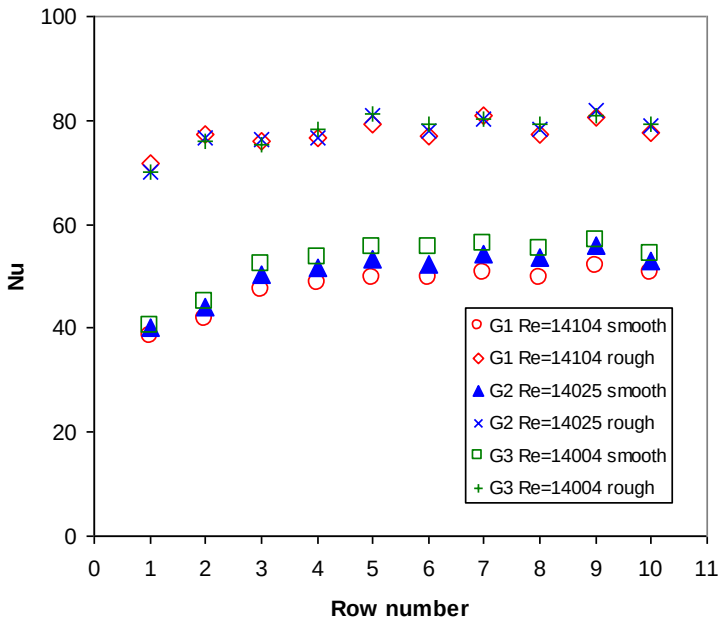

Figure 4: Local Nusselt number distributions for different grids (partial pins, G/H = 0.15).

Results

The heat transfer coefficient and Nusselt number were calculated at every row of pin fins (or channel segment) by adopting the same methodology as in the experimental analysis [7]. The heat transfer coefficient h was calculated using the difference between segment surface temperature T_s and bulk average air temperature T_b. The wall heat flux was integrated over the segment surface area. The heat transfer area A was the total area exposed to the flow, including pins and walls. T_b was determined from an energy balance from the segment location to the measured exit temperature, using the heating power downstream of the segment middle plane.

The Nusselt number was averaged over the ten segments, and is plotted against Reynolds number in Figure 5, for full pins and for partial pins with G/H of 0.15 and 0.47. The solid symbols are the experimental measurements, whereas the empty symbols are the computational predictions. The trend of the average Nusselt number for both walls in the cases of partial length pins is generally similar to that for the case with full pins. However, the magnitudes for the smooth walls are lower. The Nusselt number for the rough wall with partial length pins is comparable to that for the full pins. The numerical prediction shows good agreement with the experiments, within experimental and numerical uncertainty.

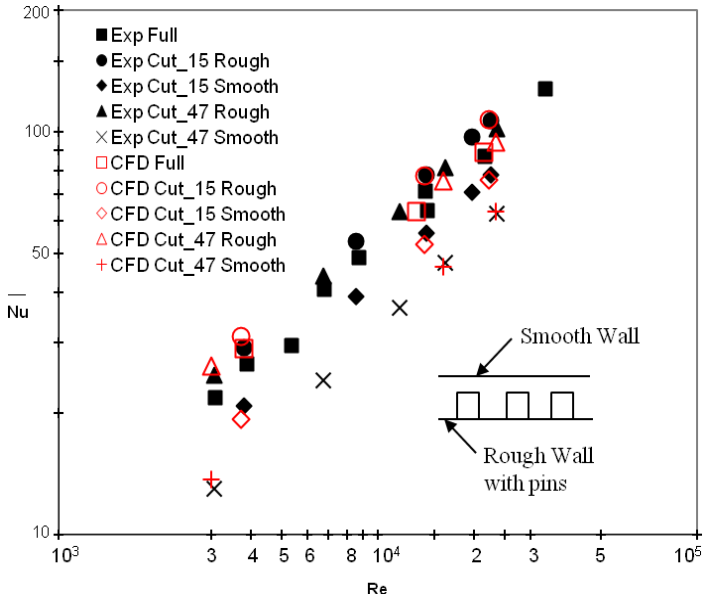

Figure 5: Nusselt number as a function of Reynolds number for the experiments and computations (full pins and partial pins with G/H = 0.15, 0.47.

CHT Analysis of a Gas Turbine Vane

Vane model

The analysed first stage turbine vane is illustrated in Figure 6, along with some of its surrounding components. It is an axial turbine configuration, with the horizontal centerline being located a distance below the domain. The vane is located directly downstream of the engine combustor. The cooling air

enters the vane through a hole in the turbine supporting case, and via a feed cavity located between the case and the vane. The vane airfoil cooling scheme is as described in Figure 1.

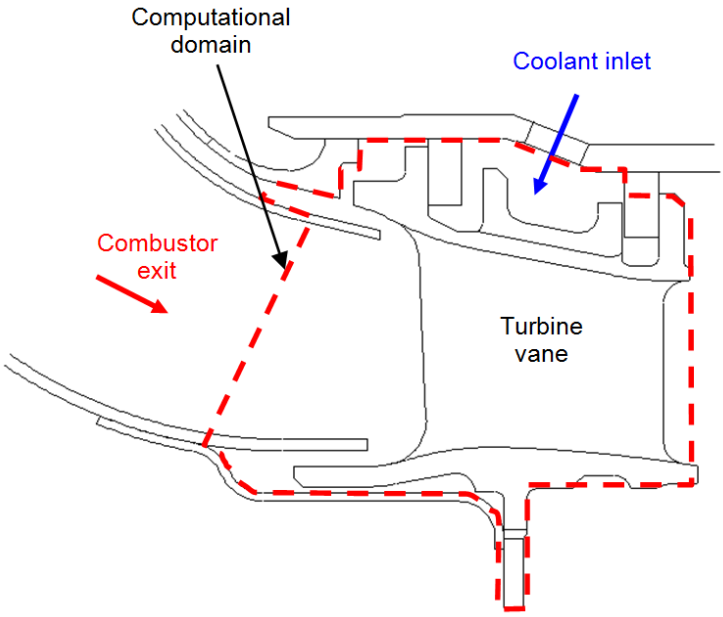

Figure 6: Analysed first stage turbine vane assembly.

Computational domain and boundary conditions

One vane airfoil was analysed only, with periodic faces defined approximately half distance to the two neighbour airfoils, in order to simulate the full circular vane arrangement. The fluid domain was composed of two regions: the hot mainstream flow surrounding the airfoil, and the internal cooling scheme. The two fluid regions were connected via the airfoil trailing edge exit slots. The inlet of the hot mainstream flow was located about half chord length upstream of the airfoil leading edge. The exit was about 11% chord length downstream from the trailing edge (see Figure 6).

The operating conditions for the analysis were set to be the same as in a thermal paint test that was conducted on the real engine. This way, direct comparison of the analytical results with the vane thermal paint readings would be possible. The operating conditions of the selected test (and analysis) are listed in Table 2.

Table 2 – Test engine and analysis operating conditions

Vane Temperature Ratio, $T_{0,in}/T_{out}$	1.28
Vane Pressure Ratio, $P_{0,in}/P_{out}$	2.20
Coolant feeding temperature, $T_{0,c}/T_{0,in}$	0.35
Coolant feeding pressure, $P_{0,c}/P_{0,in}$	0.84

Non-uniform total pressure and total temperature were specified at the mainstream inlet, simulating a hot streak coming out from the combustor. The applied dimensionless total temperature ($T_0/T_{0,in}$) profile ranges from 0.8 to 1.2, and is shown in Figure 7. The gas temperature peak was angularly aligned to strike the vane airfoil, in order to simulate the hottest possible vane condition. At the mainstream exit, a static pressure variation was specified, ranging from $P/P_{0,in}$ = 0.385 to 0.525, increasing in the radial direction. At the cooling flow inlet, total temperature and pressure were imposed.

Computational grid

A portion of the unstructured grids around the leading edge region, including the turbine vane solid domain as well as the external and internal flow domains, is shown in Figure 8. A grid sensitivity analysis was carried out for the fluid region with two grids. The mesh dependency of the predicted metal temperature distribution along the airfoil for the two different grids was inspected. The selected grid, M1, with about 6,800,000 nodes in the fluid (including cooling scheme), and a finer grid, M2, with about 11,000,000 nodes, showed only 3% difference in temperature distribution.

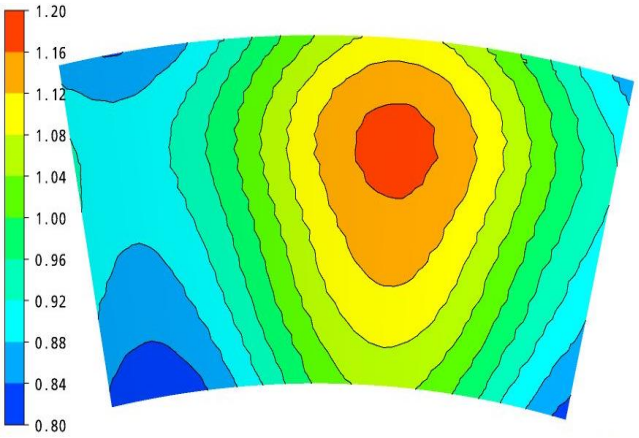

Figure 7: 2-D dimensionless total temperature ($T_0/T_{0,in}$) distribution imposed at the inlet.

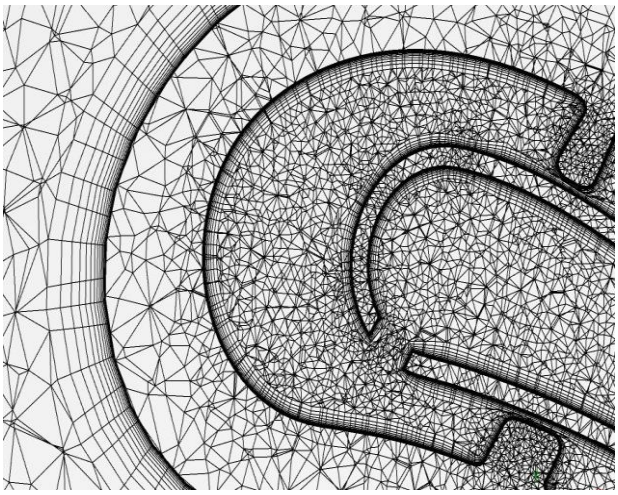

Figure 8: Cross-sectional view of the computational grid.

Solution

A converged solution was obtained after 600 iterations and 20 hours on a parallel cluster system with 24 processors. The convergence thresholds of RMS residuals for continuity, x-, y-, and z-momentums, and energy equations were set to 10^{-4}.

Results and discussion

Figure 9 shows the predicted surface metal temperature along airfoil contours at two sections of approximately constant radius. The two sections were taken at distances of 25% and 75% of the airfoil span from the vane inner shroud. The plots include the thermal paint data and the predictions of the empirical correlation based design system. The thermal paint band was obtained by averaging the readings over the six hottest airfoils of the tested vane ring, which had different types of paint on them. Three sets of CHT results were plotted: with ideal gas properties and smooth walls, with real gas

properties (Cp, k, μ varying with temperature) and smooth walls, and finally with real gas properties and roughness of 75 μin on the external surface of the airfoil.

The shape of the CHT prediction is in reasonable agreement with the thermal paint band, and this on the entire airfoil region. With the ideal gas assumption, the prediction is located around the bottom of the thermal paint band. A higher temperature distribution is obtained with the real gas model. When the surface roughness is considered, the prediction is around the top of the thermal paint band. It tends to overestimate the leading edge temperature, in comparison with the thermal paint data.

The suction side temperature is more influenced than the pressure side temperature by the surface roughness. A detailed analysis of the flow parameters near the suction side wall revealed that surface roughness made the velocity boundary layer thicker, made the thermal boundary layer thinner, and increased the turbulence intensity. Details of this analysis are skipped here for brevity. Practically, due to the test condition being analysed, i.e. a thermal paint test using a new vane, the smooth wall assumption was selected as the best one in this case. However, in cases of rougher surface vanes, like used vanes, roughness should not be neglected.

Higher temperature prediction was to be expected from the CHT simulation, compared to thermal paint readings, especially at the airfoil leading edge. The mainstream inlet hot streak was set to the highest possible temperature from the combustor, and was aligned directly onto the airfoil leading edge, which represents the worst possible airfoil condition. On the other hand, the thermal paint band came from an average of multiple airfoils that were not all exposed to the same peak temperature in the test engine.

For the empirical correlation prediction, the combustor exit pattern factor, describing the amplitude of the hot streak, was adjusted (within reasonable range) to get good agreement with the thermal paint band at the airfoil leading edge. In general, the empirical correlation tends to overestimate the metal temperature on pressure and suction sides, and to flatten out the temperature peak at the airfoil leading edge.

In Figure 10, the predicted temperature pattern on the external vane surface is shown to be in good agreement with the engine thermal paint test observations. Regions at the leading and trailing edges show the highest temperatures as indicated by the thermal paint. Temperature reduces from the leading edge up to about 45% chord length, where the cooling effect of impingement jets is evident.

Finally, the predicted average Nusselt numbers for the internal coolant passages are 17.1 and 16.2 on the pressure and suction sides, respectively, with an average of 21.3 on pin fins, and 13.1 on wall surfaces. Inside the leading edge, the average Nusselt number is 20.8. These values are comparable to those from the practical relationships for each cooling feature [9].

Conclusion

The conjugate heat transfer methodology was discussed, as applied to turbine cooling. In a first step, it was successfully validated against experimental data in the case of a cooling channel with pin fins. Computed Nusselt numbers were in good agreement with the experiments for both full and partial pin fins. In a subsequent step, CHT was used to predict the airfoil metal temperature of an internally cooled gas turbine vane, under the conditions of an engine thermal paint test that had been completed. It was found to provide better prediction than the empirical prediction tool, especially around the leading edge region. The treatment of real gas properties and external surface roughness were found to have a significant impact on predicted metal temperature.

Further validation exercises on internal cooling features, for example on impingement, are still required to confirm the higher quality of the CHT prediction. Nevertheless, the successful application of the methodology to a complete turbine component demonstrated its potential as a practical tool for designing more efficient cooling schemes, and for predicting component lives.

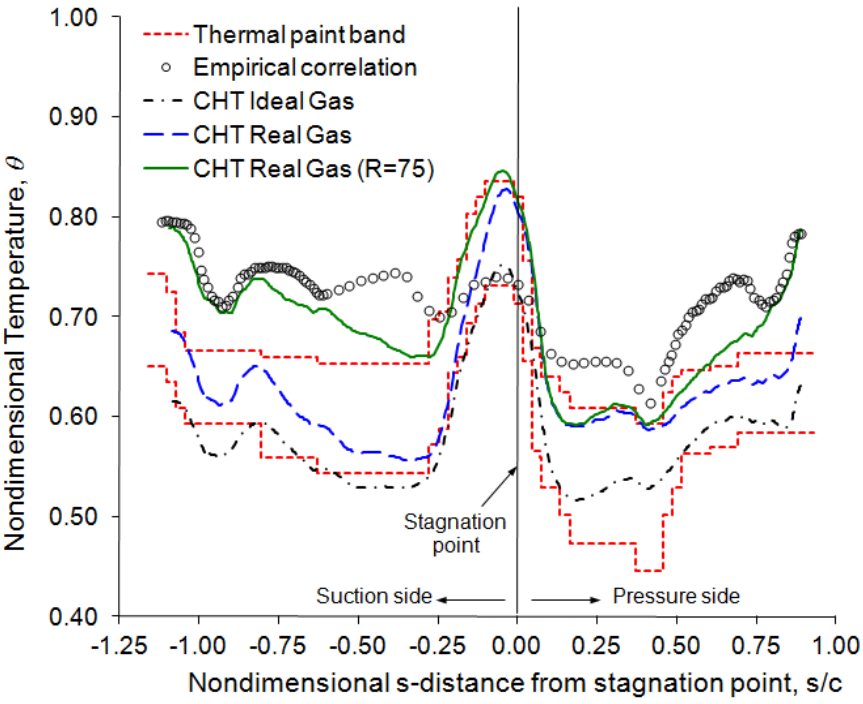

(a) 25% span

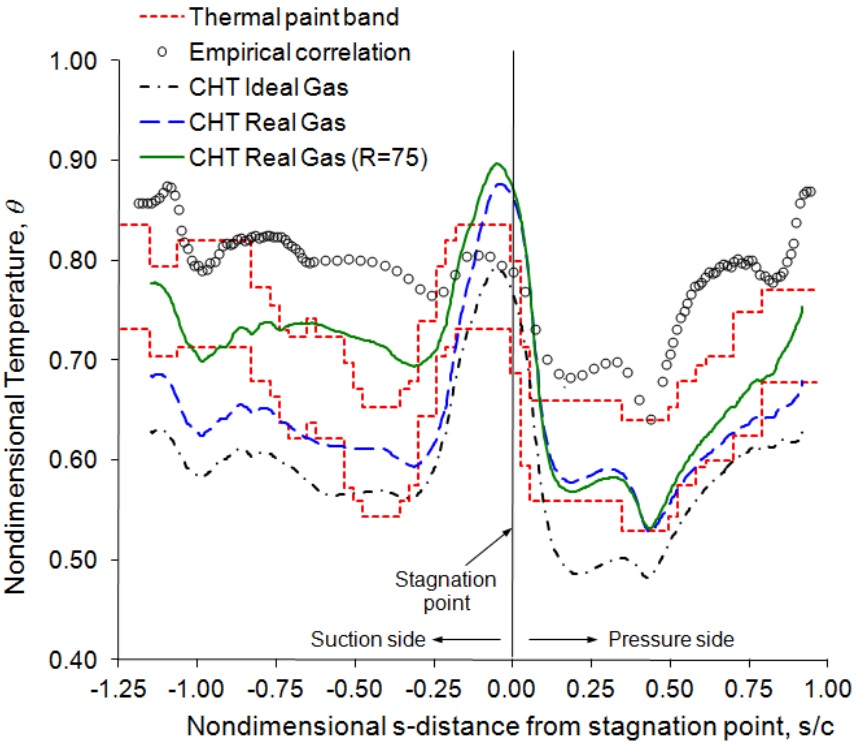

(b) 75% span

Figure 9: Surface metal temperature distributions.

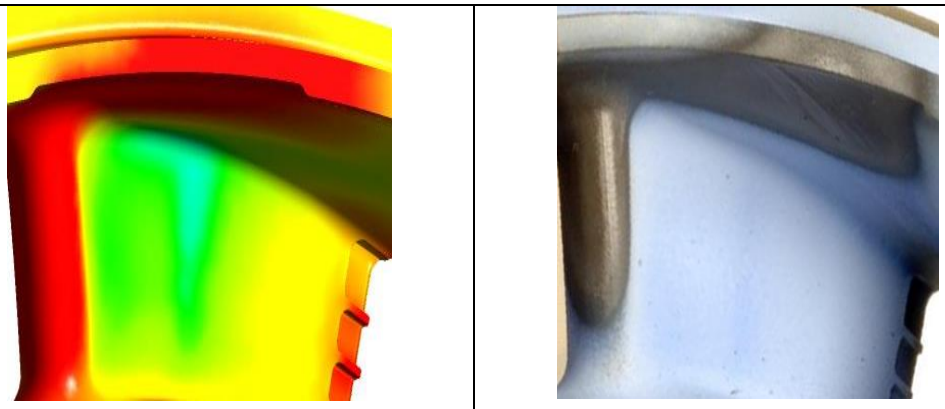

(a) CHT prediction	*(b) Thermal paint*

Figure 10: Comparison of the metal temperature prediction with the thermal paint result (airfoil pressure side view).

References

[1] Ligrani, P. M., Oliveira, M. M., and Blaskovich, T., 2003, "Comparison of Heat Transfer Augmentation Techniques," *AIAA Journal*, Vol. 41, No. 3, pp. 337-362.

[2] Heidmann, J. D., Kassab, A. J., Divo, E. A., Rodriguez, F., and Steinthorsson, E., 2003, "Conjugate Heat Transfer Effects on a Realistic Film-Cooled Turbine Vane," ASME Paper No. GT2003-38553.

[3] Mazur, Z., Hernandez-Rossette, A., Garcia-Illescas, R., and Luna-Ramirez, A., 2006, "Analysis of conjugate heat transfer of a gas turbine first stage nozzle," Applied Thermal Engineering, Vol. 26, pp. 1796-1806.

[4] Kusterer, K., Hagedorn, T., Bohn, D., and Sugimoto, T., and Tanaka, R., 2006, "Improvement of a Film-Cooled Blade by Application of the Conjugate Calculation Technique," ASME Journal of Turbomachinery, Vol. 128, pp. 572-578.

[5] Luo, J. and Razinsky, E. H., 2007, "Conjugate Heat Transfer Analysis of a Cooled Turbine Vane Using the V2F Turbulence Model," ASME Journal of Turbomachinery, Vol. 129, pp. 773-781.

[6] Ledezma, G. A., Laskowski, G. M., and Tolpadi, A. K., 2008, "Turbulence Model Assessment for Conjugate Heat Transfer in a High Pressure Turbine Vane Model," ASME paper No. GT2008-50498.

[7] Arora, S. C., and Abdel-Messeh, W., 1990, "Characteristics of Partial Length Circular Pin Fins as Heat Transfer Augmentors for Airfoil Internal Cooling Passages," ASME Journal of Turbomachinery, Vol. 112, pp. 559-565.

[8] ANSYS CFX Release 11.0, 2006.

[9] Cunha, F. J., Abdel-Messeh, W., and Chyu, M. K., 2006, "Thermal Analysis and Durability Design Strategies for Gas Turbine Airfoils," ASME paper No. GT2006-91013.